Comparison of Hot Wire TIG Stellite 6 weld cladding and lost wax cast Stellite 6 under corrosive wear conditions

F. Brownlie[1*], C. Anene[2], T. Hodgkiess[3], A. Pearson[4], A.M. Galloway[1]

1: Department of Mechanical and Aerospace Engineering, University of Strathclyde, Glasgow, UK
2: Department of Naval Architecture and Marine Engineering, University of Strathclyde, Glasgow, UK
3: Porthan Ltd, Lochgilphead, UK
4: Weir Engineering Services, East Kilbride, UK
[*]**Corresponding author:** f.brownlie@strath.ac.uk

Abstract

This study compares Hot Wire Tungsten Inert Gas Stellite 6 weld cladding on a low carbon steel substrate with a lost wax cast Stellite 6 in impingement erosion-corrosion conditions. Austenitic stainless steel samples were used as a reference material. Tests were conducted in a closed loop impinged slurry vessel with a jet velocity of 18m/s with 3.5%NaCl aqueous solution containing 500 micron spherical silica sand particles (0.5g/l sand concentration). The testing temperature was 40°C. Mass loss measurements and a volumetric analysis as well as microstructural evaluation were used as post-test analysis techniques. Results showed that weld cladding and lost wax cast Stellite 6 performed better than the stainless steel, with the weld cladding marginally outperforming the lost wax cast technique.

1. Introduction

Corrosive wear can occur when water impinges or flows over a surface. The severity of the corrosive wear increases with the suspension of solid particles. The material degradation is caused by mechanical wear from the solid particles and by electrochemical corrosion processes. This type of wear is a major issue to a variety of engineering applications such as pipe lines, piping components, pump impellers and casings. If this complex phenomenon is not taken into consideration when designing and implementing engineering systems then the consequences may lead to poor performance and ultimately component failure.

The complexity of erosion-corrosion has been studied in the past [1–4] and it has been found that there are three main degradation mechanisms. The pure mechanical damage (M) is attributed to erosion and abrasion from the sand particles, the pure corrosion (C) is caused by electrochemical reactions and synergy (S) is caused by the interaction between the erosion and corrosion damage.

An enhanced volumetric analysis technique has been developed which further evaluates erosion-corrosion phenomena [5]. This technique separates the two different wear zones, Directly Impinged Zone (DIZ) and Outer Area (OA), found in the impinged jet test apparatus which is utilised in this study. The mechanical degradation mechanisms (impingement erosion and sliding abrasion) along with the electrochemical processes and their synergistic effects can be quantified in both wear regions during solid-liquid impingement conditions.

One way of alleviating erosion-corrosion damage is to reduce the effect of the electrochemical corrosion process. This can be done by using corrosion resistant alloys (CRA). These are a group of alloys that produce a thin passive oxide film which helps to create a barrier against corrosion and is a strategy that is widely used for surgical implant materials [6] and offshore components [7]. One such alloy is Stellite 6 (UNS R30006). This has a cobalt based matrix with a chromium carbide hard phase and is commonly used for components which experience highly erosive and corrosive environments.

Slurry jet erosion [6-7], slurry pot [6,8], cavitation erosion [9-10] and pin on disk [11-12] are some of the various testing methods which have been used to demonstrate the corrosion and wear resistance of Stellite alloys. A study conducted by Neville and Hodgkiess [9] was conducted on Stellite 6 at a perpendicular impingement angle in solid-liquid conditions. The corrosion resistance of the Stellite 6 was poor compared to Inconel 625 and Superduplex stainless steel; however, the Stellite 6 demonstrated the best wear resistance of the three tested materials. Studying the effects of different angles of impingement is important as industrial components such as piping and pumping systems will experience erosive particles impacting at a range of impact angle. This type of study was performed by Andrews et al. [15] who assessed the effect of impingement angle on Stellite 6 that had been cast by two different methods, sand casting and lost wax casting. It was found that the Stellite 6 castings were most susceptible to erosion-corrosion damage at 60° angle of impingement. The Stellite 6 castings performed better than austenitic stainless steel (UNS S31600) at all angles of impingement and both casting techniques performed very similarly in all testing conditions. Erosion-corrosion testing conducted on Stellite x40 has shown that it also has good corrosive wear resistance, if the solid particle loading is low [14–16].

Stellite alloys with the addition of molybdenum were found to have better erosion-corrosion resistance than Stellite alloys with added tungsten due to the molybdenum forming secondary carbides[19]. Another study found that Stellite alloys with tungsten have good corrosion resistance in oxidising conditions whereas, Stellite alloys with molybdenum have good corrosion and wear resistance in reducing environments[20]. The dry sliding wear, solid particle wear and corrosion performance of Stellite 21 alloys with higher molybdenum content was studied by Liu et al. The intermetallic compound formed by the additional molybdenum was found to increase the sliding wear resistance and had similar corrosion resistance as the basic Stellite 21 alloy however, the intermetallic compound was found to reduce its solid particle erosion resistance [21].

Hot Isostatic Pressed (HIPed) Stellite 6 was found to have significantly better impact toughness and contact fatigue when compared to a cast Stellite 6. This was attributed to the finer microstructure produced by the HIPed process [22]. Malayoglu and Neville [23] also found a slight improvement in terms of erosion-corrosion resistance of the HIPed process over casting of Stellite 6.

CoCrMo alloys are also used extensively in the biomedical industry for metal-on-metal hip implant joints; hence, the tribocorrosion mechanisms of these alloys have been studied extensively [24–27]. In these tribocorrosion (sliding wear with corrosion) conditions the CoCrMo alloys were observed to experience chemical wear (wear accelerated corrosion) and mechanical wear [28]. Some studies have also assessed the effect of simulated biological environments on the tribocorrosion process of CoCrMo alloys [29–31]. These studies observed that the proteins present in the simulated biological fluid generates a protective layer on the surface of the CoCrMo alloys and causes a boundary lubrication effect. This results in reduced friction in the tribocorrosion system.

Clearly, a potentially advantageous way of obtaining the material properties of Stellite 6, at reduced overall component cost, is through deposition onto a substrate via a cladding process [32, 33] and potentially in the future through a cold gas spraying process [34]. In this respect, there have been some investigations of laser cladding of Stellite alloys. Singh et al. found that Stellite 6 laser claddings significantly improved the corrosion, cavitation and solid particle erosion of a 14Cr-4Ni stainless steel [35]. Another study by Shin et al. discovered that the dry abrasion resistance of a Plasma Transferred Arc Stellite 6 weld cladding improved as the molybdenum content was increased [36]. There currently has been little or no work conducted on assessing the corrosive wear resistance of Stellite 6 weld claddings.

This present study comprises an assessment of the erosion-corrosion performance of Stellite 6 hot wire tungsten inert gas (HWTIG) weld cladding on a low carbon steel substrate in comparison with lost wax cast Stellite 6. This will consider whether there are any differences in corrosive wear performance between a single or double HWTIG layers in addition to determining if a weld cladding can perform comparably to a cast material. Erosion-corrosion testing was conducted with an impinging saline aqueous solution jet at normal incidence (90°) for 1 hour. Austenitic stainless steel (UNS 31600) was used as a reference material to benchmark the Stellite 6 alloys.

2. Methodology and Materials

2.1 Methods

Before conducting erosion-corrosion testing, the materials were initially characterised using light microscopy (Olympus GX51) and Scanning Electron Microscopy (SEM - Hitachi SU-6600) with a 20kV accelerating voltage and secondary electron detector. Phase identification was conducted using a Bruker AXS-D8 Advance X-ray diffractometer using Cu Kα radiation. The scanning range was from 35° to 100° at a scan step size of 0.05° and time of 0.5s at 40kV and 40mA.

The erosion-corrosion testing consisted of two different experiments, liquid impingement and solid-liquid impingement tests. The testing apparatus utilised in this study (Figure 1) is of similar design as discussed previously [37]. The liquid impingement test was conducted in a recirculating impingement apparatus with a 3.5% NaCl aqueous solution with a jet velocity of 18m/s and a nozzle of 3.8mm. The solid-liquid impingement testing was conducted with a 3.5%NaCl aqueous solution with 500 micron spherical silica sand (1160Hv) with a sand concentration of 0.5g/l. The test duration was 1 hour. The sand size distribution was measured by sieving the sand incrementally by way of fine sieves; the sand size distribution is given in Table 1. The jet was submerged and had a velocity of 18m/s and a nozzle diameter of 3.8mm. The nozzle was consistently offset from the specimen surface by 5mm. The test temperature range for the solid-liquid impingement tests was 37-40°C. Solid-liquid impingement tests were also conducted with cathodic protection in order to provide information on the material degradation mechanisms occurring on the tested materials.

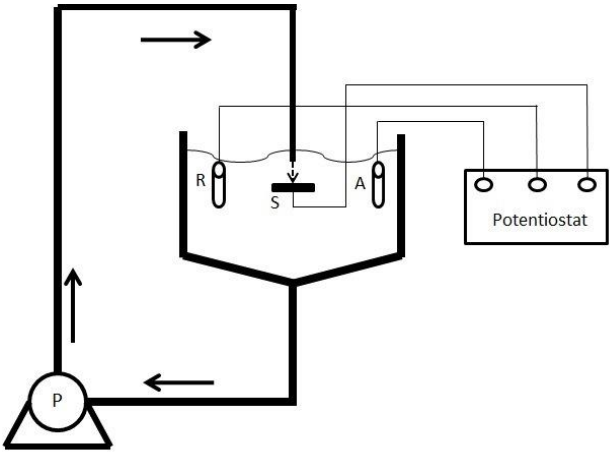

Figure 1: Schematic of erosion-corrosion test rig

Table 1: Particle size distribution of spherical silica sand

Particle Size (μm)	Percentage (%)
≤ 250	2.5
250-420	18.4

421-500	50.7
501-600	23.3
≥ 601	5.1

All specimens were ground before polarisation and erosion-corrosion testing by using silicon carbide papers from 220 – 1200 grit. Specimens were weighed before each test on a mass balance with an accuracy of ±0.1mg. After each liquid impingement test, the medium carbon steel was submerged in an inhibited acid solution (Clarks Solution) to remove the extensive corrosion product. Post-test analysis was also conducted using an Alicona Infinite Focus 3D optical profilometer with a wear scar volume accuracy of ±0.02mm^3. A Mituyoto SV-2000 2D surface profilometer was used for roughness measurements. Macro-hardness measurements were conducted using a Vickers hardness testing apparatus with a 5kgf load.

Potentiodynamic scans were conducted to assess the electrochemical corrosion rates in static, liquid impingement and solid-liquid impingement conditions. The potentiodynamic scans were conducted 15 minutes after the sample was submerged to allow for the free corrosion potential, E_{corr}, to stabilise. Gill AC electrochemical monitoring equipment was utilised for the potentiodynamic polarisation and cathodic protection tests. Platinum was used for the auxiliary electrode and Ag/AgCl was used as the reference electrode. Polarisation tests were conducted by shifting the initial electrode potential either 20mV more positive (cathodic) or 20mV more negative (anodic) than the free corrosion potential, hence ensuring that the transition point would occur. Scans were then made 300mV more negative (for cathodic scans) or 300mV more positive (for anodic scans) at a sweep rate of 15mV/min which has been widely used by other researchers [23, 38, 39]. This sweep rate is slightly greater than the ASTM standard rate of 10mV/min [40] but any differences between the two sweep rates would be highly unlikely to effect the polarisation behaviour of the test materials. The chosen ranges were sufficient to evaluate corrosion current measurements by way of Tafel extrapolation. The measured current densities were then used to evaluate the associated mass losses due to corrosion via calculation by Faraday's Law. To conduct the polarisation tests, an electrically conductive wire was connected to the rear of the specimens, which were then cold mounted in epoxy resin. For the cathodic protection experiments, the electrode potential was maintained at -800mV (Ag/AgCl) at which potential back extrapolation of the anodic polarisation curves demonstrated that residual anodic reaction rates were negligible.

2.2 Materials

The materials tested in this study were a lost wax cast Stellite 6, HWTIG single and double layer Stellite 6 weld cladding on a low carbon steel substrate (UNS G43400), UNS G10400 and UNS S31600. The macro-hardness measurements for all test materials are given in Table 2.

Table 2: Macro-hardness values for each test material

Material	Hardness (HV)
Lost Wax cast Stellite 6	402
Single layer Stellite 6 weld cladding	401
Double layer Stellite 6 weld cladding	440
SS316	200

The microstructure of the single and double layer Stellite 6 as well as the lost wax cast Stellite 6 after polishing and etching is shown in Figure 2. Both the lost wax cast Stellite 6 and the weld deposited Stellite 6 have a typical dendritic type structure with a hypoeutectic

microstructure. The microstructure contains primary Co-rich dendrites (light grey areas) which are surrounded by Cr-rich eutectic carbides (dark grey areas) in a solid solution cobalt-rich matrix. It is noticeable that both weld claddings had smaller and finer dispersed carbides compared to the lost wax cast Stellite 6. A small percentage of tungsten-rich phases (white regions) are also present in both microstructures. A commercial vendor conducted the chemical analysis of the single and double layer Stellite 6 weld claddings as well as the lost wax cast Stellite 6 using standard chemical analysis techniques. The chemical analysis of the tested materials, the nominal composition of the feedstock used for HWTIG process as well as the low alloy steel substrate and stainless steel alloys are given in Table 3. The depths of the single and double layer weld deposits were measured using Image J software on cross sections and were found to be 1.4mm and 3.1mm respectively.

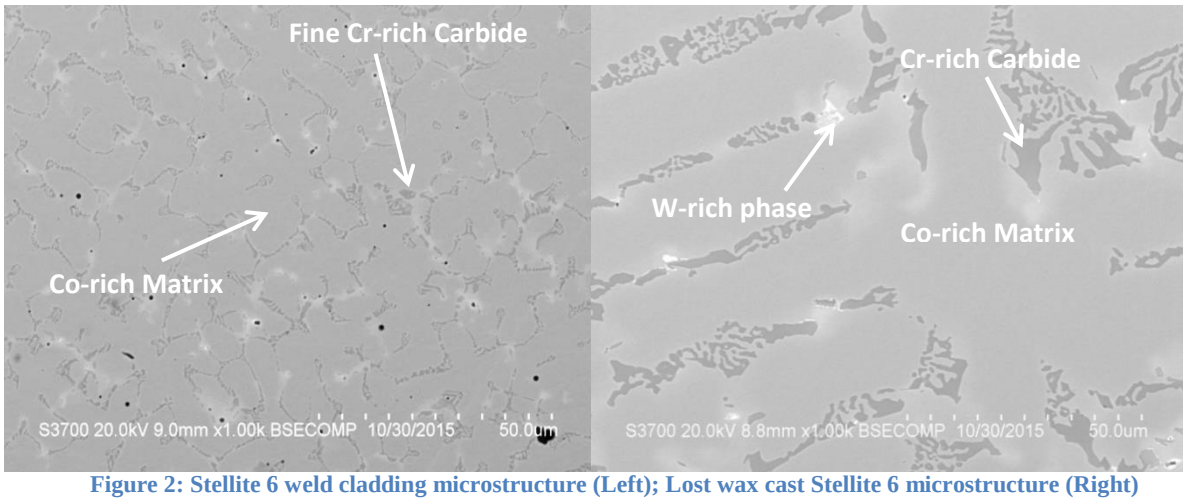

Figure 2: Stellite 6 weld cladding microstructure (Left); Lost wax cast Stellite 6 microstructure (Right)

Table 3: Chemical composition of feedstock welding rod (nominal), measured chemical composition of Stellite 6 alloys and the nominal chemical composition of the low alloy steels and stainless steels

Material	Si	Cr	Mn	Fe	Co	Ni	Mo	W	C
Feedstock	2.00	30.0	0.50	3.00	Bal.	3.00	1.00	5.00	1.20
Single Layer Weld Cladding	0.99	23.2	0.92	20.7	Bal.	0.04	0.02	3.89	0.89
Double Layer Weld Cladding	1.13	24.2	0.93	18.2	Bal.	0.04	0.02	3.76	0.90
Lost Wax Cast	0.85	29.0	0.28	2.66	Bal.	1.92	0.69	4.77	1.13
UNS S31600	0.75	18.0	2.00	Bal.	-	14.00	3.00	-	0.08
UNS G43400	-	0.9	0.80	Bal.	-	2.00	0.30	-	0.43
UNS G10400	-	-	0.90	Bal.	-	-	-	-	0.44

The chemical analysis indicates that the chromium, nickel, molybdenum and tungsten contents of the clad layers are all reduced compared to the feedstock and lost wax cast. There has also been an increase in manganese and iron in the Stellite 6 weld claddings. These alterations in the chemical composition occur due to the welding process, as the high temperatures associated with welding, melt the substrate which mixes with the molten hardfacing material before solidifying. Therefore, the first layer of the Stellite 6 weld claddings will contain higher proportion of elements directly from the low alloy steel substrate (mainly iron). The second deposited layer melts and mixes only with the first

deposited layer; hence, the double layer weld cladding contains more chromium and less iron (i.e. closer to the feedstock material). As chromium, nickel and molybdenum are well known to increase the corrosion resistance of a material then the weld dilution might be expected to reduce the corrosion resistance of the Stellite 6 weld claddings. The XRD examinations (Figure 3) did not identify any substantial difference between cast and weld clad materials, the presence of Co, Cr_3C_2 and Co W was observed as major phases in all three materials. Minor peaks were evident for $Cr_{21}W_2C_6$ and Co Fe in both weld deposits but not so in the cast Stellite 6.

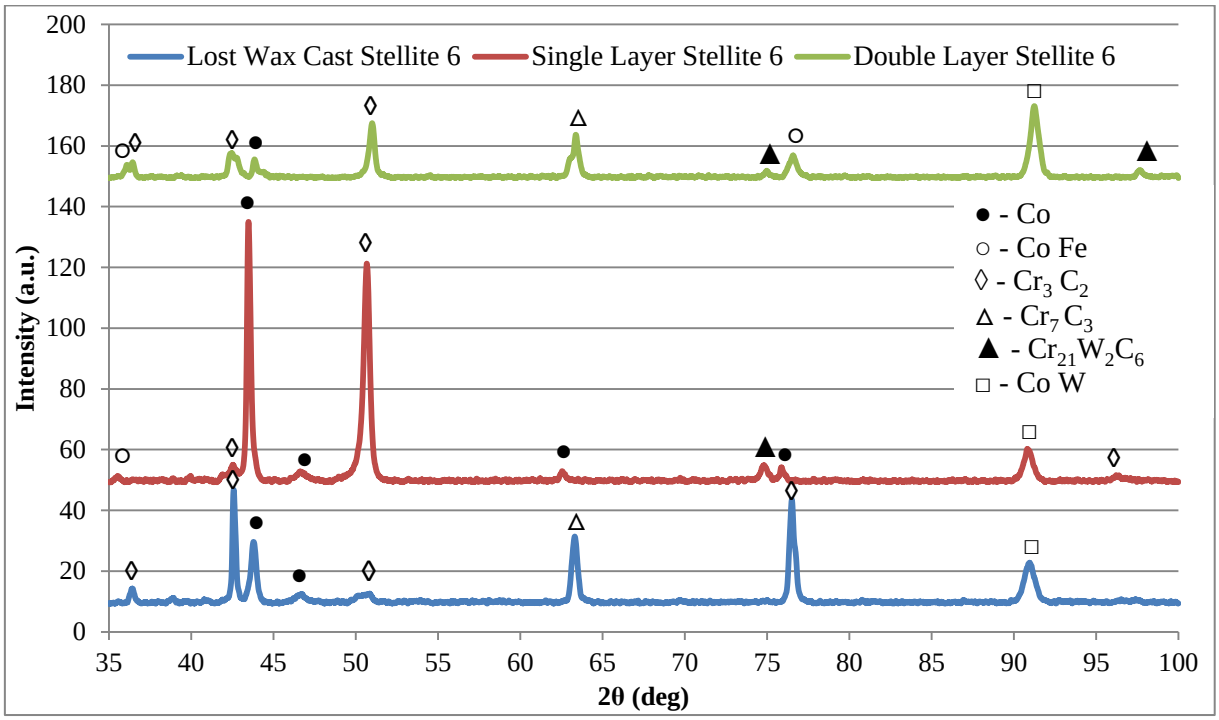

Figure 3: XRD patterns for lost wax cast Stellite 6, single layer Stellite 6 and double layer Stellite 6

The single and double layer weld cladding specimens had a diameter of 38mm which resulted in a test area of 11.34cm^2. The lost wax cast Stellite 6 had a surface test area of 6.25cm^2. A reference material of UNS S31600 (of both surface test sizes) was used to correlate the results. Despite the difference in testing areas, it is shown that this mismatch in area size did not affect the interpretation of the results (as can be seen in Results section 3.2). For liquid impingement tests, a medium carbon steel (UNS G10400) was also tested to highlight the superior corrosion resistance of the CRA's.

3. Results

3.1 Liquid impingement testing

The liquid impingement tests were conducted on single and double layer weld cladding Stellite 6, UNS S31600 and UNS G10400. At least two replicates were conducted for each material. Results from these tests are given in Figure 4.

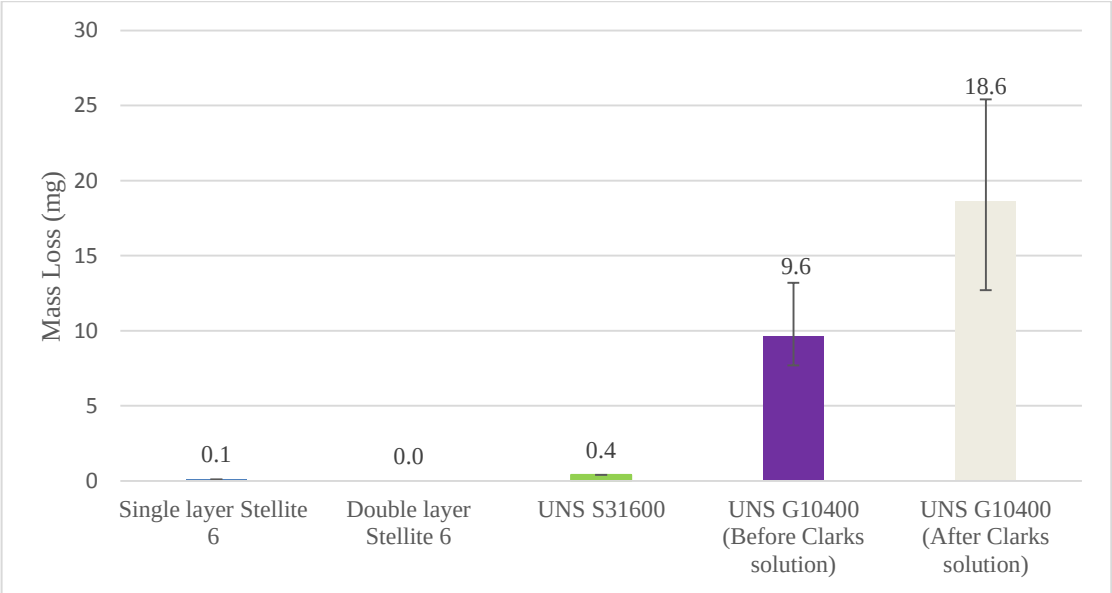

Figure 4: Average mass Losses for each material under liquid impingement conditions

From the results, it can be seen that both Stellite 6 weld cladding layers and the UNS S31600 showed virtually no mass loss in the liquid erosion-corrosion test. This shows that CRA's such as Stellite 6 and UNS S31600 demonstrate very good corrosion resistance even under liquid impingement conditions as the average mass loss value was less than 0.5mg. There was no detected scatter in the results from the Stellite 6 and UNS S316000 specimens. The UNS G10400 had a high mass loss even before immersing in Clarks solution to remove corrosion products as shown in Figure 4. A wide range in scatter was found in the UNS G10400 samples due to the poor corrosion resistance of the material.

3.2 Solid-liquid impingement testing

Solid liquid erosion-corrosion tests were conducted on single and double layer weld cladding Stellite 6 circular (11.34cm^2) specimens, lost wax cast Stellite 6 square (6.25cm^2) specimens and UNS S31600 (circular and square shaped specimens). At least 3 replicates of material were conducted to assess the experimental scatter in the testing procedure. Results for free erosion-corrosion (FEC) and Impressed Current Cathodic Protection (ICCP) are shown in Figure 5.

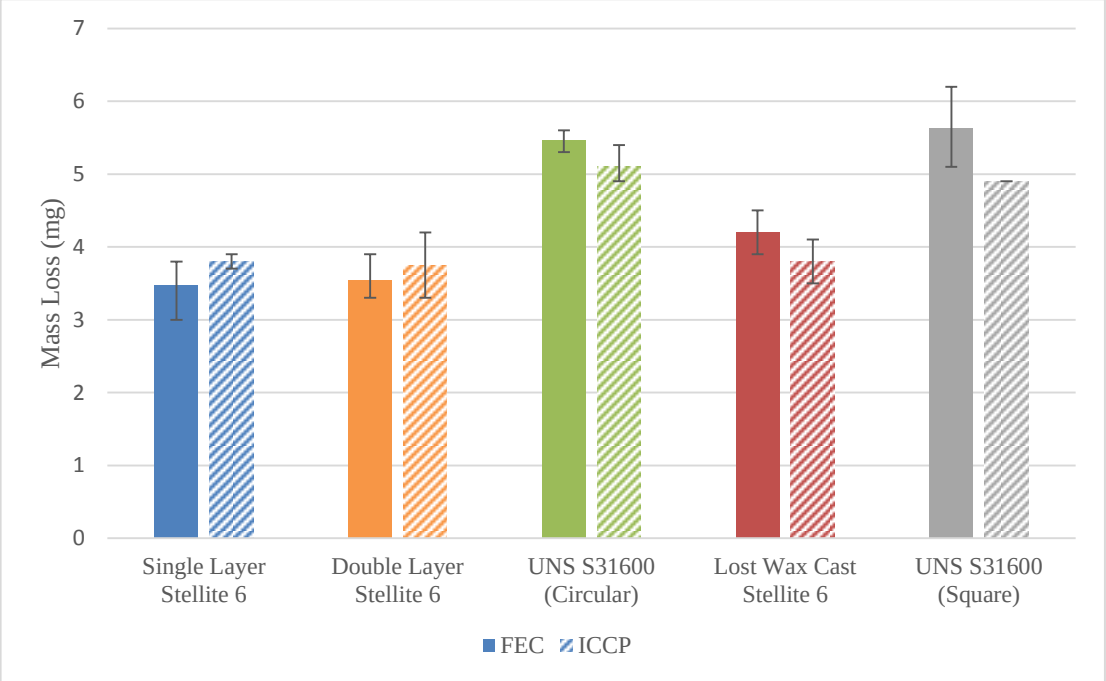

Figure 5: Average mass losses under solid liquid FEC and ICCP tests

Both UNS S31600 samples had similar mass losses in both FEC and ICCP conditions, despite their difference in size and shape. As demonstrated from visual and microscopic evidence, presented (Section 3.3) later; this was due to negligible damage occurring in the outer regions of the larger-area specimens. Therefore, it was possible to compare all samples directly. In FEC conditions, the single and double layer UNS R30006 weld cladding performed slightly better than the cast Stellite 6. The UNS S31600 stainless steel specimens showed a higher average mass loss than the Stellite 6 alloy specimens under FEC and ICCP test conditions. In all cases (except the UNS S31600 square) the scatter bands between FEC and ICCP conditions overlap. Consequently no influence arising from the application of cathodic protection could be discerned. No scatter was found in the UNS S31600 stainless steel (square) samples during ICCP tests.

3.3 Potentiodynamic tests

Anodic and cathodic polarisation scans were conducted on single and double layer weld cladding Stellite 6, lost wax cast Stellite 6 and UNS S31600 stainless steel (circular) samples. Tests were conducted in-situ in static conditions, liquid impingement and solid liquid impingement conditions. The results are illustrated in Figures 6-8 where the free corrosion potential values (listed in Table 4) have been normalised to zero volts in order to facilitate an easier comparison of the various polarisation curves.

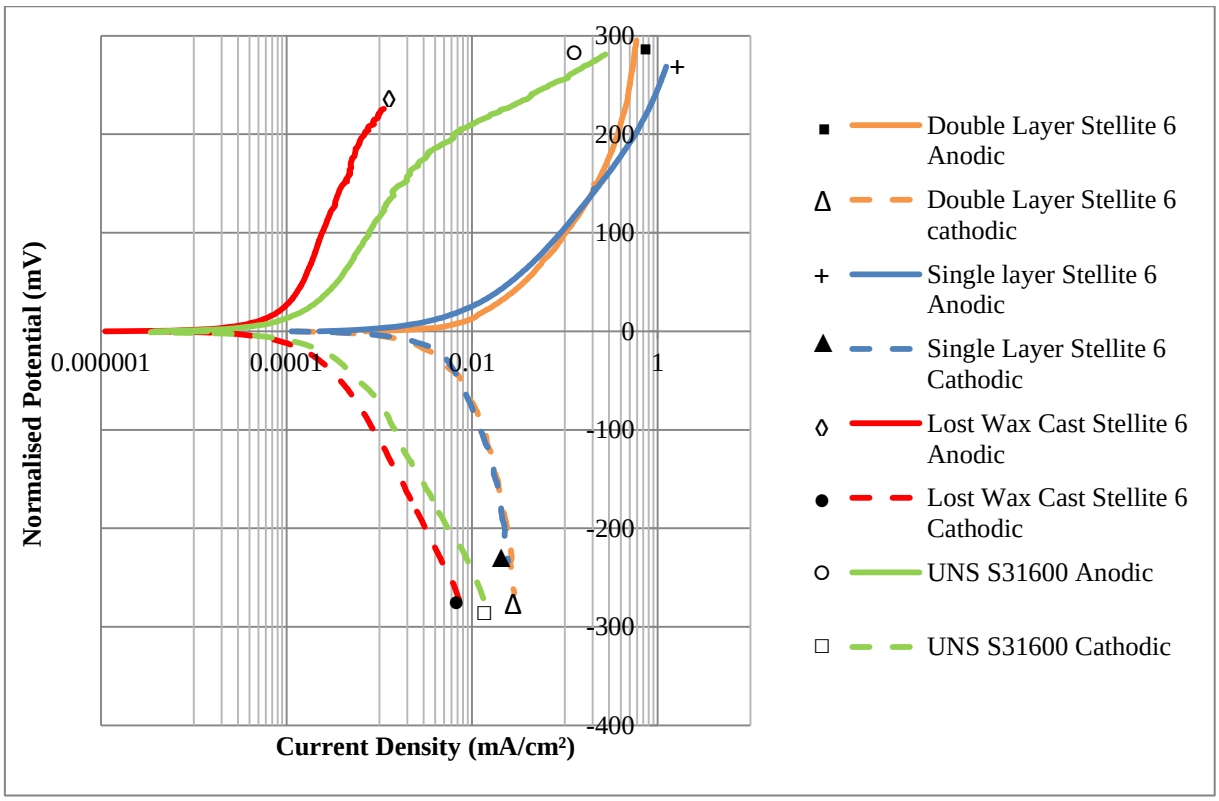

Figure 6: Anodic and cathodic polarisation plots for tested materials under static conditions

The results from the polarisation curves (Figure 6) in static conditions indicate stable oxide films for the UNS S31600 and lost wax cast Stellite 6 with both weld cladded Stellite 6 specimens exhibiting rather higher electrochemical activity under static conditions as can be seen from the extrapolated corrosion current density and associated mass loss (Table 5). The UNS S31600 stainless steel specimen exhibited some indication of a breakdown in its passive film (signalled by a more rapid increase in current) in the potential region of 120 to 200 mV positive to E_{corr}. The lost cast wax specimen demonstrated the lowest electrochemical activity (i.e. more protective behaviour) under static conditions.

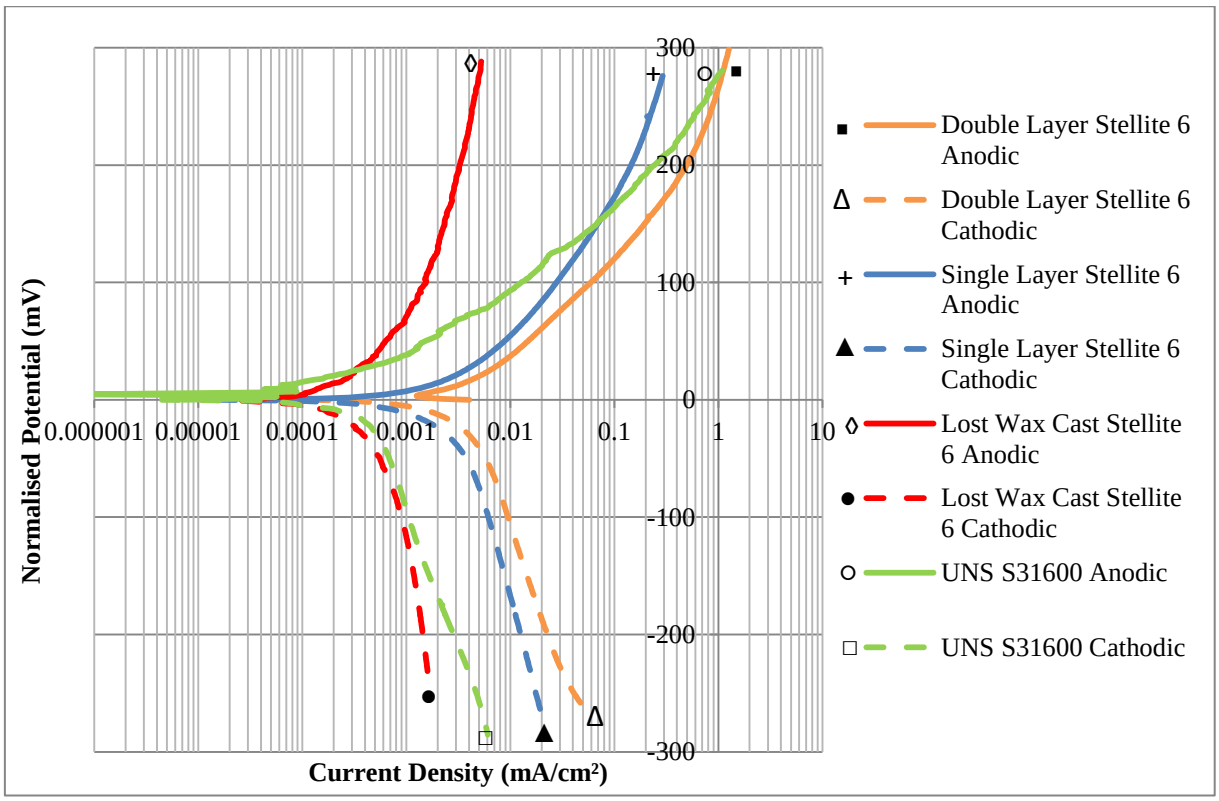

Figure 7: Anodic and cathodic polarisation plots for tested materials under liquid impingement conditions

Comparison between Figures 6 and 7 shows that the trend of the four materials in the anodic and cathodic polarisation curves were similar under static and liquid impingement conditions. However, with the weld cladded Stellite 6 test specimens there was a notable decrease in the extrapolated corrosion current density in liquid impingement conditions compared to static conditions (Table 5).

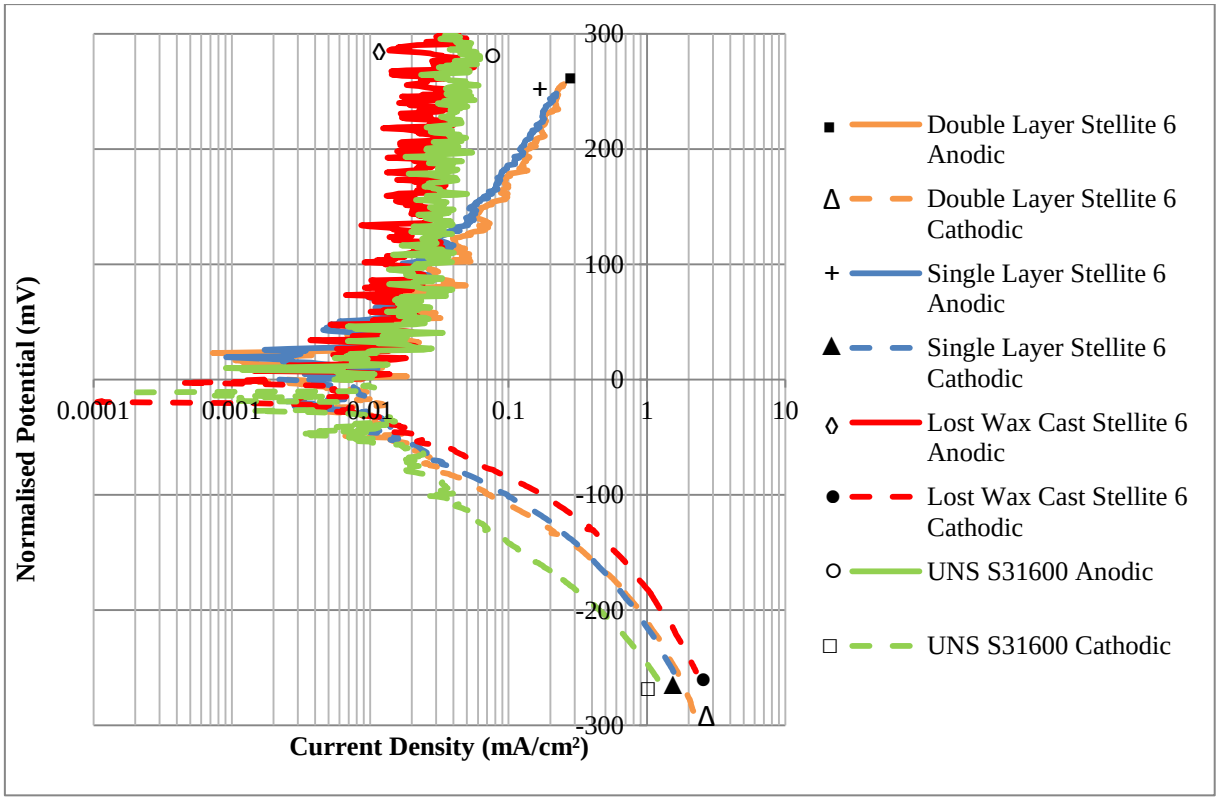

Figure 8: Anodic and cathodic polarisation plots for tested materials under solid-liquid impingement conditions

Under solid-liquid conditions (Figure 8), visible oscillations can be observed from the anodic polarisation curves of all the test specimens indicating periodic de-passivation/re-passivation events. The oscillations can still be seen at the initial points on the cathodic polarisation curve. This behaviour is attributed to the impacting solid particles and accompanying electrochemical transients associated with cyclic formation and breakdown of the passive film occurring over the wear regions.

Table 4: Free corrosion potentials (E_{corr}) for all materials in each testing environment

Material	E_{corr} – Static Conditions	E_{corr} – Liquid impingement conditions	E_{corr} – Solid-liquid conditions
Double layer Stellite 6	-460mV	-443mV	-532mV
Single layer Stellite 6	-465mV	-447mV	-479mV
Lost wax cast Stellite 6	-250mV	-114mV	-546mV
UNS S31600	-187mV	-101mV	-504mV

The trends for the free corrosion potential (Table 4) in static and liquid impingement conditions are similar with the single and double layer Stellite 6 demonstrating the most negative potentials and the UNS S31600 illustrating less negative potentials indicating the different corrosion rates in these conditions. However, in solid-liquid conditions, all materials have similar free corrosion potentials which indicate that the materials are corroding at similar rates. These trends are in line with the corrosion current densities given in Table 5.

A comparison of the corrosion rates in the three conditions is presented in Table 5. The values represent averages of electrochemical monitoring exercises conducted in triplicate. Generally, the corrosion rates for each material increased as the environment became more aggressive. The lost wax cast Stellite 6 demonstrated the smallest corrosion mass loss in each environment, whereas, the weld cladded Stellite 6 illustrated the highest corrosion rate and associated mass loss in all testing conditions. Nevertheless, the calculated mass loss of 0.15mg/hr for the weld clad material equates only to roughly 0.01mm/yr thickness loss. It should also noted that the damage associated with corrosion in this study is small (less than 0.4mg, which is approximately 10% of the total erosion-corrosion damage). Therefore, the testing conditions of this experimental study is erosion dominated.

Table 5: Corrosion current density measurements and associated mass loss for tested materials

Material	Corrosion Current Density (mA/cm^2) Static Condition	Mass Loss (mg/hr) Static Condition	Corrosion Current Density (mA/cm^2) Liquid Impingement Condition	Mass Loss (mg/hr) Liquid Impingement Condition	Corrosion Current Density (mA/cm^2) Solid-Liquid Impingement Condition	Mass Loss (mg/hr) Solid-Liquid Impingement Condition
Double Layer Stellite 6	0.01	0.15	0.006	0.089	0.024	0.35
Single	0.01	0.15	0.004	0.059	0.023	0.18

Layer Stellite 6						
Lost Wax Cast Stellite 6	0.00016	0.0013	0.0005	0.0040	0.023	0.18
UNS S31600	0.00021	0.0010	0.00057	0.0028	0.019	0.22

3.3 Post-test examination

Macroscopic and microscopic observation was undertaken after the solid-liquid impingement tests. Figure 9 shows the various zones which are created on the test specimens during 90^{o} angle of impingement tests.

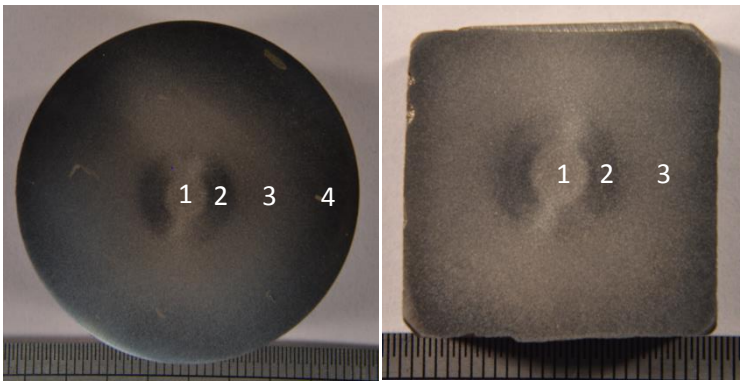

Figure 9: Post-test images of Weld cladding Stellite 6 (Left) and lost wax cast Stellite 6 (Right) after solid-liquid impingement

These various material degradation regions are:

- Zone 1 – Direct Impinged Zone (DIZ)
- Zone 2 – Turbulent Zone
- Zone 3 –Visually damaged outer area
- Zone 4 – Outermost area exhibiting negligible damage

For all tested materials, the majority of damage occurred in the direct impingement zone (this is illustrated for one material in zone 1 – Figure 10) where the impact of particles develops small pits and craters. Zones 2 and 3 experience sliding abrasion degradation as a result of grazing impact at low impacting angles (<10°). There was minimal damage in the outermost area (zone 4) which can be microscopically observed from Figure 13.

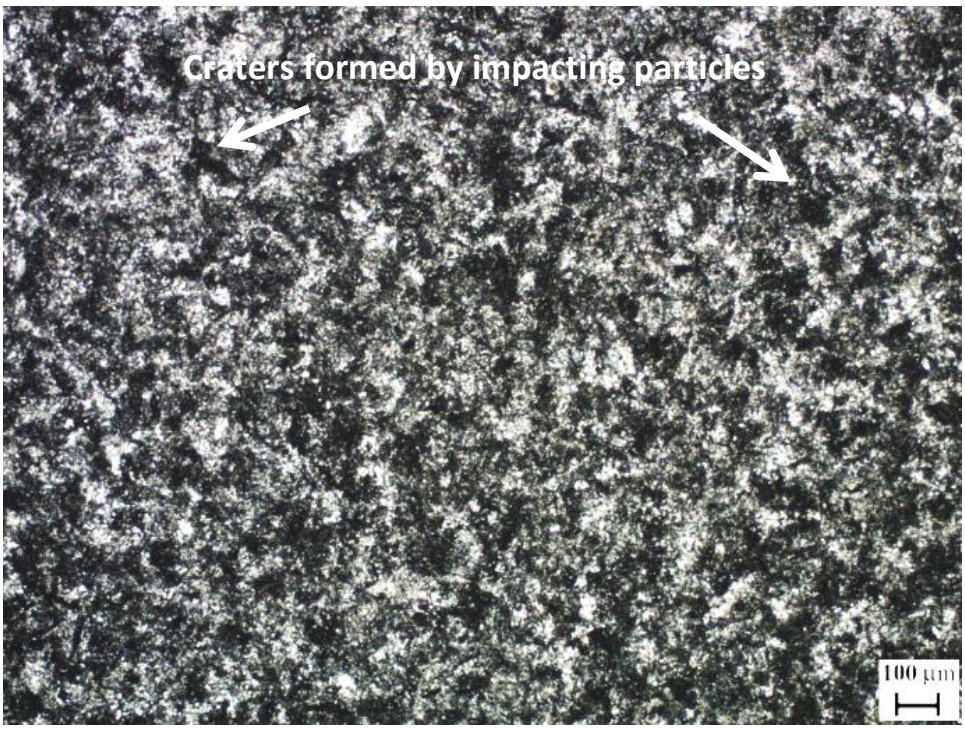

Figure 10: Surface damage in zone 1 (DIZ) – weld cladding Stellite 6

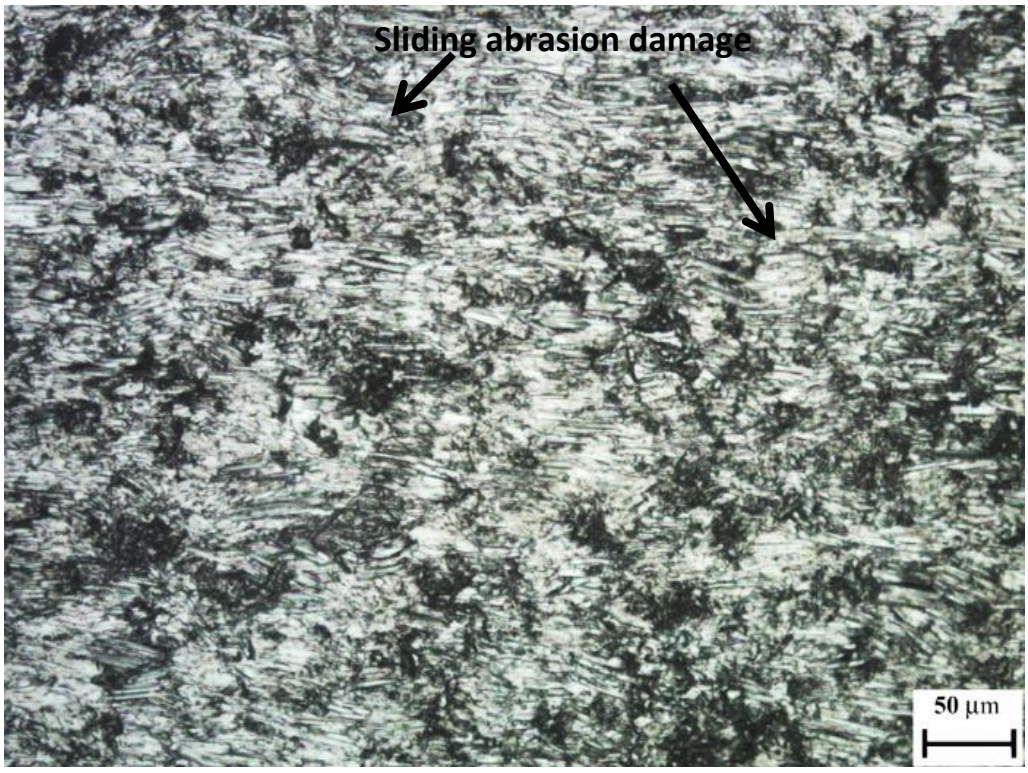

Figure 11: Surface damage in Zone 2 (turbulent zone) – weld cladding Stellite 6

Zone 2 (Figure 11) is the turbulent region directly adjacent to the DIZ. The majority of the damage found in this region is sliding abrasion damage which can be seen with the directional markings on the surface. The darker regions in the microstructure have also experienced sliding abrasion damage; however, small craters have formed due to material loss, which has allowed corrosion to commence in these areas. Hence, this is possible evidence of synergy occurring in this region. These dark regions can also be seen in zone 3 (Figure 12). Sliding abrasion damage is the main material degradation mechanism occurring in this region.

Figure 12: Surface damage in Zone 3 (Outer Area) – weld cladded Stellite 6

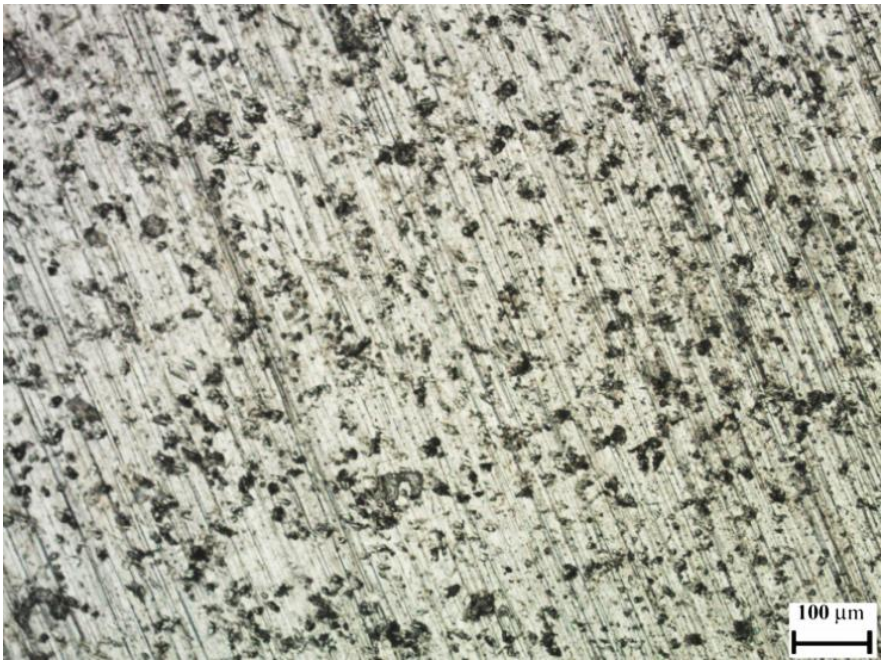

Figure 13: Minimal surface damage in zone 4 – weld cladding Stellite 6

The outermost region (zone 4) experiences the least amount of damage compared to the other zones as the particulates have lost most of their kinetic energy at this stage. However, some particles do impact on the surface resulting in the small dark regions (Figure 13), which were similar to the dark regions found in zones 2 and 3. Pre-test grinding marks are visible (top left corner to bottom right corner).

The damaged areas observed on all test specimens were confined within a surface area of $6\pm0.2cm^2$. Observation of the lost wax cast Stellite 6 specimen (Figure 9) confirms this, where even the outer edges of the specimen show damage due to sliding abrasion. The outermost zone for the circular (larger surface area) specimens indicate virtually no damage (Figure 13).

Thus there were no significant effects on the experimental results from the use of the square samples for test comparison (as indicated in mass loss measurements, Figure 5).

Although the damage incurred by the different materials was similar, in order to quantify the damage occurring in each zone, surface roughness measurements were assessed. Measurements were taken from a single layer weld cladding and a lost wax cast sample. A minimum of three measurements were taken in each zone. As the lost wax cast did not have an outermost region (zone 4) then measurements were not possible. Results indicate that the roughness in each zone decreased as the zones became further away from the impinged jet [37]. This indicates that the surface damage becomes less severe further from the wear scar. A significant difference in roughness was observed in zone 1 between the weld cladding and the lost wax cast. This indicates that the lost wax cast Stellite 6 is less resistant in turbulent conditions. However, in all other regions the roughness values were similar. It should be noted that the roughness of the materials before testing was 0.07µm Ra. This indicates that there is minimal damage occurring in Zone 4.

Table 6: Surface roughness of the different zones after solid-liquid impingement tests

Material	Zone 1, Ra (µm)	Zone 2, Ra (µm)	Zone 3, Ra (µm)	Zone 4, Ra (µm)
Weld cladding Stellite 6	1.74	0.28	0.24	0.13
Lost Wax Cast Stellite 6	3.01	0.29	0.25	*

* No outer zone observed

3.4 Volumetric analysis

Volumetric analysis was undertaken to assess the volume loss of the test materials in the direct impingement zone. Figure 14 shows the volume loss measurement of the direct impingement zone of a UNS S31600 specimen taken after a FEC test. The analysis was taken inside the region of the superimposed red ring which represents the zone directly under the impinging fluid.

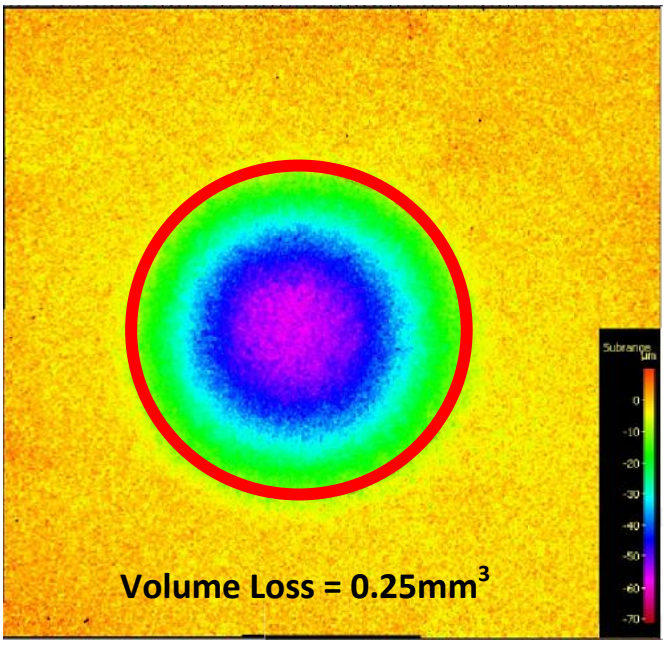

Figure 14: Volumetric analysis of the direct impinged zone of a UNS S31600 specimen after solid liquid impingement test

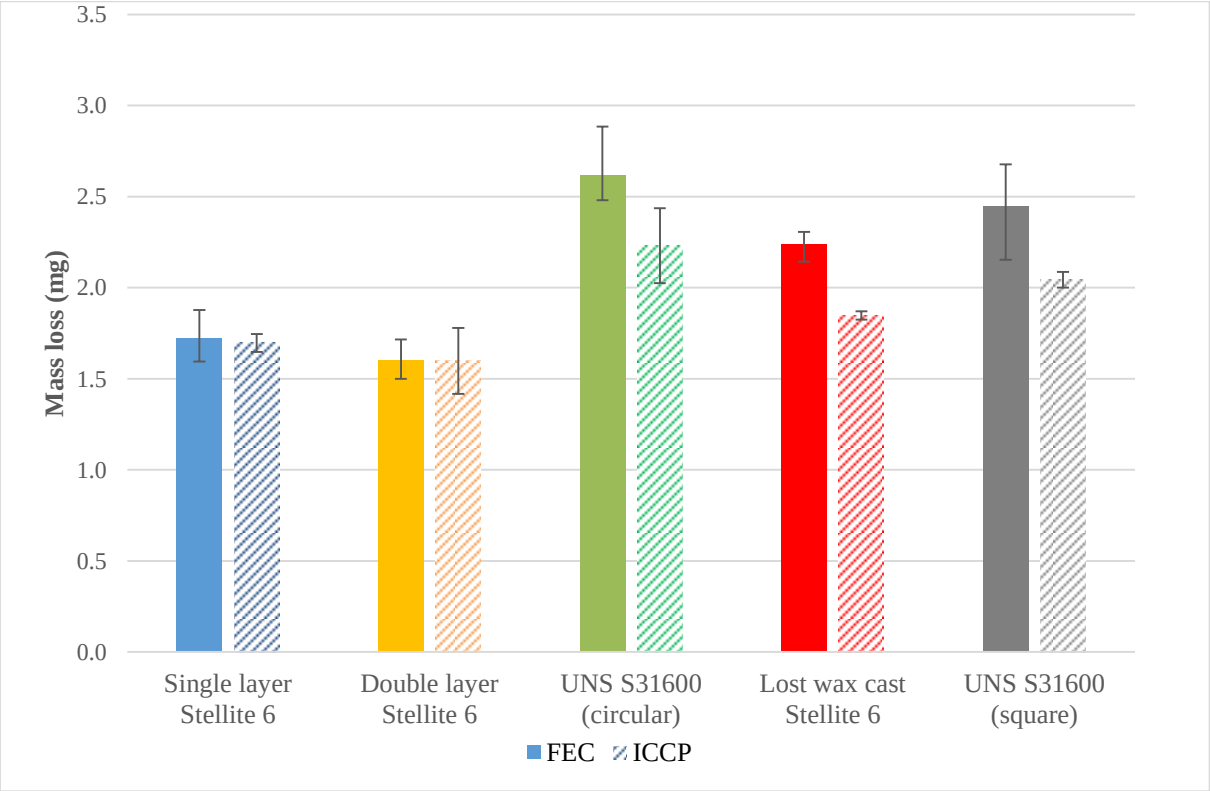

Figure 15: Average mass loss in the DIZ for each tested material in FEC and ICCP conditions

Figure 155 illustrates the average mass losses (converted from volume loss) of the tested materials within the direct impinged zone with and without cathodic protection. There was no clear reduction in DIZ mass loss under cathodic protection in the weld clad Stellite 6 specimens but a reduction was evident in the lost wax cast Stellite 6 and UNS S31600 specimens. This trend is in line with the result from the total mass losses of the materials from ICCP testing illustrated in Figure 5.

A volumetric analysis technique [5] was also utilised to provide further evaluation of the inherent corrosive wear resistance of the tested materials. Mass losses for the two distinct wear zones (directly impinged zone – "DIZ" and the outer area – "OA") can be by converting the measured DIZ volume losses to mass losses via the known density (8.4 g/cm²) of Stellite 6 followed by subtraction from the measured total mass loss.

Figure 16 illustrates the mass losses occurring in the two different wear regions, the DIZ and the OA. The mass losses in the DIZ were found to be smaller for the Stellite 6 weld claddings when compared to both the lost wax cast Stellite 6 and UNS S31600 materials. In terms of the mass loss in the OA, there was no difference between the Stellite 6 weld claddings and the lost wax cast Stellite 6. The UNS S31600 materials demonstrated significantly greater mass losses in the OA compared to Stellite 6.

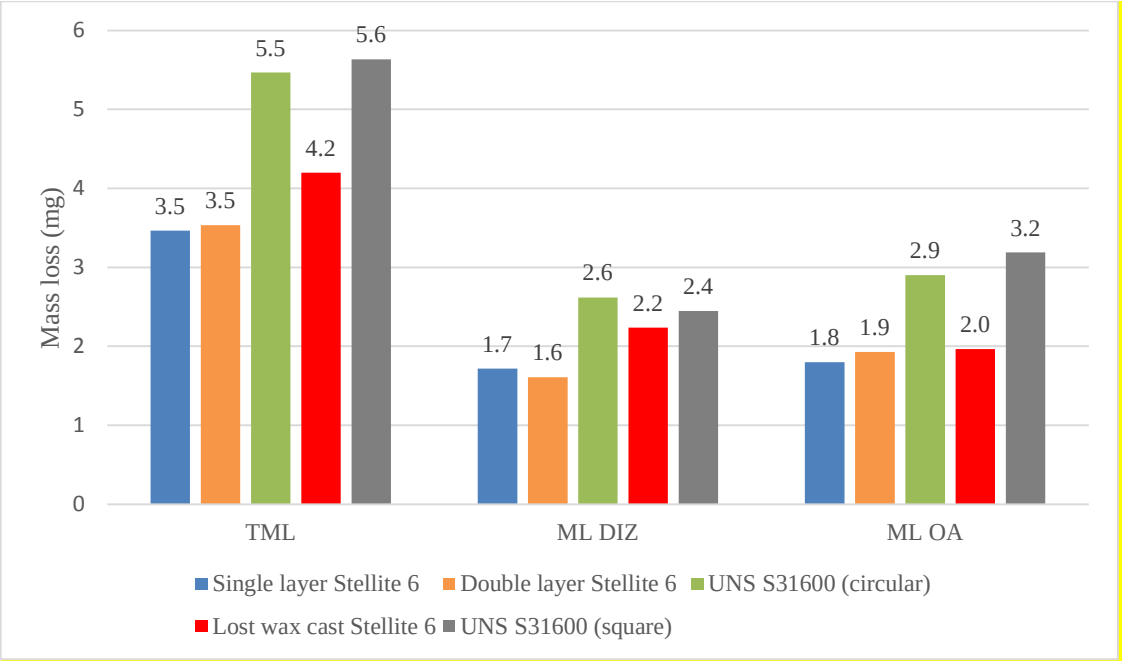

Figure 16: Breakdown of the mass losses in the two distinct wear zones in FEC conditions

4. Discussion

A number of interesting aspects have been highlighted by this comparative study between the HWTIG process and lost wax casting process of Stellite 6. From metallurgical examination, the microstructure of the Stellite 6 was very similar with both processes demonstrating the typical hypoeutectic microstructure of Co-rich matrix surrounded by Cr-rich eutectic carbides [41]. A small quantity of substantially sized inclusions (2-3 per test coupon) were observed (Figure 17) on the top surface of the weld claddings. SEM spot analysis indicated that these impurities were Co-rich (>94%). It is postulated that these inclusions are a result of contaminated feedstock material and/or poor control of the welding process. Despite these defects being apparent in the weld clad materials, they did not drastically affect their overall corrosive wear behaviour. From an industrial context, the results from this study implies that there may be a degree of tolerance to welding defects in engineering components experiencing corrosive wear conditions.

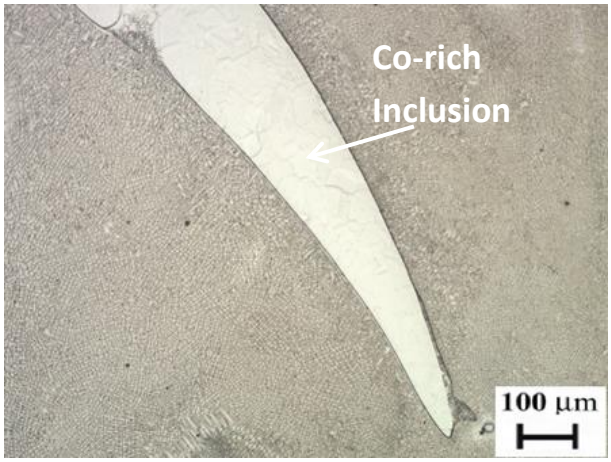

Figure 17: Inclusion found on top surface of the single layer weld cladding Stellite 6

The Stellite 6 and stainless steel both exhibited excellent erosion-corrosion resistance in liquid impingement conditions, as would be expected [16]. This was also evident from the high mass loss (Figure 4) of the low alloy steel attributed to its poor corrosion resistance. However,

there was a clear difference between the lost wax cast Stellite 6 and the HWTIG Stellite 6 during electrochemical polarisation tests in the different test environments. In static and liquid impingement conditions, the Stellite 6 weld cladding had a significantly greater corrosion rate than the lost wax cast Stellite 6. This can be attributed to the weld dilution effect which has caused chromium, nickel and molybdenum (chemical elements well known for increasing the corrosion resistance of a material) to be diffused from the weld cladding into the substrate, shown in Table 3. As only a maximum of two welding passes were performed, the nominal chemical composition of Stellite 6 could not be achieved. Hence, the lost wax cast Stellite 6 demonstrated better corrosion resistance during polarisation testing. However, as corrosion effects are small in this study (contributing to approximately less than 10% of the overall damage), then the difference in chemical composition has less effect in erosion-corrosion conditions, as shown in Figure 5.

The expanded post-test volumetric analysis has shown that the relevant performance of various materials is dependent upon the type of wear mechanisms. The Stellite 6 weld claddings appear to possess higher resistance to *direct impingement* damage than the lost wax cast Stellite 6. However, the weld claddings and lost wax cast Stellite 6 perform similarly in the outer area where sliding abrasion is the predominant mechanism. In this wear region, the stainless steel is most vulnerable. These findings are in accordance with the generally accepted notion that material hardness dictates to a large extent, resistance to abrasion. The slightly lower material loss of the Stellite 6 weld claddings in the DIZ may be associated with the finer chromium carbides observed in the microstructure (Figure 2) although the presence of the $Cr_{21}W_2C_6$ as a minor phase may also be a contributory factor (Figure 3). Improvement in wear resistance by having finer chromium carbides in the microstructure has been found in a previous study [42]. There also seemed to be no difference between the performance of the single and double layer weld claddings as they have similar chemical composition and microstructure.

The improvements in wear resistance for Stellite 6 claddings compared to stainless steels have been observed in past studies. Singh et al. found that Stellite 6 laser cladding performed better than 13Cr-4Ni stainless steel in solid particle erosion tests [35]. Another study by Romo et al. observed that a Shielded Metal Arc Welded (SMAW) Stellite 6 coating performed slightly better than a 13Cr-4Ni stainless steel in 5 minutes slurry erosion tests [43]. The findings of the current study represent evidence of good durability in somewhat different environmental conditions than the previous work, but, perhaps more importantly, demonstrates that the weld cladded Stellite 6 displays equivalent or better erosion-corrosion resistance than the cast form of the material.

For the majority of the test materials, there was no significant benefit of applying cathodic protection; hence the majority of the damage was mechanical. However, it was observed that there was a slight increase in average mass loss for the Stellite 6 weld claddings when cathodic protection was applied. A possible explanation for greater mass losses during cathodic protection is the possibility of localised hydrogen embrittlement mechanisms. Any involvement of hydrogen embrittlement would be expected to be more pronounced at the more negative electrode potential at which hydrogen production cathodic reactions are accelerated. To examine this possibility, cathodic protection tests were conducted on single layer Stellite 6 weld cladding at a range of electrode potentials (-700mV, -800mV and -900mV) each test had two replicates. Table 7 demonstrates that the mass losses were similar for each electrode potential and that the average mass loss at all electrode potentials were equal to or less than the average mass loss in FEC conditions.

Table 7: Comparison of mass losses of single layer Stellite 6 weld cladding at different cathodic potentials

Single Layer Stellite 6 Weld Cladding	CP (-700mV)	CP (-800mV)	CP (-900mV)	FEC
Mass Loss 1 (mg)	3.5	3.2	3.2	
Mass Loss 2 (mg)	3.3	3.8	3.0	
Average Mass Loss (mg)	3.4	3.5	3.1	3.5

As mass losses in FEC and CP conditions were within experimental scatter and as the mechanical wear processes (erosion and sliding abrasion) are the main material degradation processes, then it is clear (in the context of this study) that there is no benefit in applying CP to the Stellite 6 materials.

5. Conclusions

- Although the electrochemical corrosion rates of the weld deposited Stellite 6 were greater than those of Stellite 6 cast and SS316 in static and high velocity saline water in the absence of solid particles, the actual corrosion rates were extremely low. This in accordance with the measured total mass losses in which the performance of the weld deposited Stellite 6 essentially matched the (expected) high resistance of the chromium containing alloys which is indicative of stable passive oxide films.
- Under solid-liquid impingement conditions, the total mass loss measurements indicates that the weld clad Stellite 6 experienced similar (or slightly lower) material loss than either cast Stellite 6 or SS316. The additional data obtained using the volumetric analysis technique demonstrated that the benefit of weld cladding was mainly associated with superior resistance under direct impingement rather than the sliding abrasion wear encountered in the outer region of the test specimens.
- The resistance of weld cladded Stellite 6 was likely to be related to the finer carbide particles compared to the lost wax cast Stellite 6. The presence of Co-rich inclusions on the top surface of the weld cladded Stellite 6 did not appear to affect the erosion-corrosion behaviour.
- Application of impressed current cathodic protection yielded no discernible differences in material loss. This demonstrated that the degradation of the materials under the conditions of this study was dominated by mechanical damage rather than corrosion processes. Nevertheless, the corrosion related damage amounted to about 5-10% of total material loss.

Overall, the assessment from the experimental tests and results shows that cladding by HWTIG using Stellite 6 alloy performs similarly, if not better, with the corrosive wear performance of a cast Stellite 6 alloy and a stainless steel. Hence, in an industrial context, weld cladded Stellite 6 can be a cost effective method in improving the service life of components having to withstand corrosive wear conditions.

Acknowledgements

The authors would like to acknowledge the support for this study, which was provided by the Weir Group PLC (WARC2011- SAA1, 2011) via its establishment of the Weir Advanced Research Centre (WARC) at the University of Strathclyde.

References

[1] S. Aribo, R. Barker, X. Hu, and A. Neville, "Erosion–corrosion behaviour of lean duplex stainless steels in 3.5% NaCl solution," *Wear*, vol. 302, no. 1–2, pp. 1602–1608, 2013.

[2] A. Neville, T. Hodgkiess, and J. T. Dallas, "A study of the erosion-corrosion behaviour of engineering steels for marine pumping applications," *Wear*, vol. 186–187. pp. 497–507, 1995.

[3] R. J. K. Wood, J. C. Walker, T. J. Harvey, S. Wang, and S. S. Rajahram, "Influence of microstructure on the erosion and erosion-corrosion characteristics of 316 stainless steel," *Wear*, vol. 306, no. 1–2, pp. 254–262, 2013.

[4] G. T. Burstein and K. Sasaki, "Effect of impact angle on the slurry erosion–corrosion of 304L stainless steel," *Wear*, vol. 240, no. 1–2, pp. 80–94, 2000.

[5] L. Giourntas, T. Hodgkiess, and A. M. Galloway, "Enhanced approach of assessing the corrosive wear of engineering materials under impingement," *Wear*, vol. 338–339, pp. 155–163, 2015.

[6] A. Neville and Y. Yan, "Biotribocorrosion: Surface interactions in total joint replacement (TJR)," in *Tribocorrosion of Passive Metals and Coatings*, 2011, pp. 337–367.

[7] R. Johnson and C. B. Von Der Ohe, "Tribocorrosion in marine environments," in *Tribocorrosion of Passive Metals and Coatings*, 2011, pp. 441–474.

[8] M. Jones and R. J. Llewellyn, "Assessing the Erosion Corrosion Properties of Materials for Slurry transportation and processing in the oil sands industry," *Nace Int. Corros. 2007 Conf. expo*, no. 7685, pp. 1–15.

[9] A. Neville and T. Hodgkiess, "Characterisation of high-grade alloy behaviour in severe erosion-corrosion conditions," *Wear*, vol. 233–235, pp. 596–607, 1999.

[10] G. Nelson, G. Powell, and V. Linton, "Investigation of the wear resistance of high chromium white irons," *... ASM Int. Mater. ...*, 2006.

[11] S. Hattori and N. Mikami, "Cavitation erosion resistance of stellite alloy weld overlays," *Wear*, vol. 267, no. 11, pp. 1954–1960, 2009.

[12] M. Lee, Y. Kim, Y. Oh, Y. Kim, S. Lee, H. Hong, and S. Kim, "Study on the cavitation erosion behavior of hardfacing alloys for nuclear power industry," *Wear*, vol. 255, no. 1–6, pp. 157–161, 2003.

[13] L. Benea, P. Ponthiaux, F. Wenger, J. Galland, D. Hertz, and J. . Malo, "Tribocorrosion of stellite 6 in sulphuric acid medium: electrochemical behaviour and wear," *Wear*, vol. 256, no. 9–10, pp. 948–953, 2004.

[14] H. So, C. T. Chen, and Y. a Chen, "Wear behaviours of laser-clad stellite alloy 6," *Wear*, vol. 192, pp. 78–84, 1996.

[15] N. Andrews, L. Giourntas, A. . Galloway, and A. Pearson, "Effect of impact angle on the slurry erosion-corrosion of Stellite 6 and SS316," *Wear*, vol. 320. pp. 143–151, 2014.

[16] A. Neville, M. Reyes, T. Hodgkiess, and A. Gledhill, "Mechanisms of wear on a Co-base alloy in liquid–solid slurries," *Wear*, vol. 238, pp. 138–150, 2000.

[17] M. Reyes and A. Neville, "Degradation mechanisms of Co-based alloy and WC metal–matrix composites for drilling tools offshore," *Wear*, vol. 255, no. 7–12, pp. 1143–1156, 2003.

[18] A. Neville, H. Xu, and M. Reyes, “Corrosion and erosion-corrosion behavior of a Co-based alloy and a Ni-containing austenitic cast iron,” *Corrosion*, no. 149, p. Paper No.00031, 2000.

[19] U. Malayoglu and A. Neville, “Mo and W as alloying elements in Co-based alloys—their effects on erosion–corrosion resistance,” *Wear*, vol. 259, no. 1–6, pp. 219–229, 2005.

[20] M. X. Yao, J. B. C. Wu, and Y. Xie, “Wear, corrosion and cracking resistance of some W- or Mo-containing Stellite hardfacing alloys,” *Mater. Sci. Eng. A*, vol. 407, no. 1–2, pp. 234–244, 2005.

[21] R. Liu, J. Yao, Q. Zhang, M. X. Yao, and R. Collier, “Effects of molybdenum content on the wear/erosion and corrosion performance of low-carbon Stellite alloys,” *Mater. Des.*, vol. 78, pp. 95–106, 2015.

[22] H. Yu, R. Ahmed, H. D. V. Lovelock, and S. Davies, “Influence of Manufacturing Process and Alloying Element Content on the Tribomechanical Properties of Cobalt-Based Alloys,” *J. Tribol.*, vol. 131, no. 1, p. 11601, 2009.

[23] U. Malayoglu and A. Neville, “Comparing the performance of HIPed and Cast Stellite 6 alloy in liquid–solid slurries,” *Wear*, vol. 255, no. 1–6, pp. 181–194, 2003.

[24] R. Büscher, G. Täger, W. Dudzinski, B. Gleising, M. A. Wimmer, and A. Fischer, “Subsurface microstructure of metal-on-metal hip joints and its relationship to wear particle generation,” *J. Biomed. Mater. Res. - Part B Appl. Biomater.*, vol. 72, no. 1, pp. 206–214, 2005.

[25] A. Igual Muñoz and S. Mischler, “Effect of the environment on wear ranking and corrosion of biomedical CoCrMo alloys,” *J. Mater. Sci. Mater. Med.*, vol. 22, no. 3, pp. 437–450, 2011.

[26] H. Mishina and M. Kojima, “Changes in human serum albumin on arthroplasty frictional surfaces,” *Wear*, vol. 265, no. 5–6, pp. 655–663, 2008.

[27] S. Mischler and A. I. Muñoz, “Wear of CoCrMo alloys used in metal-on-metal hip joints: A tribocorrosion appraisal,” *Wear*, vol. 297, no. 1–2, pp. 1081–1094, 2013.

[28] S. Guadalupe, S. Cao, M. Cantoni, W. J. Chitty, C. Falcand, and S. Mischler, “Applicability of a recently proposed tribocorrosion model to CoCr alloys with different carbides content,” *Wear*, vol. 376–377, pp. 203–211, 2017.

[29] Y. Yan, A. Neville, D. Dowson, and S. Williams, “Tribocorrosion in implants-assessing high carbon and low carbon Co-Cr-Mo alloys by in situ electrochemical measurements,” *Tribol. Int.*, vol. 39, no. 12, pp. 1509–1517, 2006.

[30] Y. Yan, A. Neville, and D. Dowson, “Tribo-corrosion properties of cobalt-based medical implant alloys in simulated biological environments,” *Wear*, vol. 263, no. 7–12, pp. 1105–1111, 2007.

[31] M. T. Mathew, M. J. Runa, M. Laurent, J. J. Jacobs, L. A. Rocha, and M. A. Wimmer, “Tribocorrosion behavior of CoCrMo alloy for hip prosthesis as a function of loads: A comparison between two testing systems,” *Wear*, vol. 271, no. 9–10, pp. 1210–1219, 2011.

[32] S. Sun, Y. Durandet, and M. Brandt, “Parametric investigation of pulsed Nd: YAG laser cladding of stellite 6 on stainless steel,” *Surf. Coatings Technol.*, vol. 194, no. 2–3, pp. 225–231, 2005.

[33] M. Zhong, W. Liu, K. Yao, J. Goussain, C. Mayer, and A. Becker, “Microstructural evolution in high power laser cladding of Stellite 6+WC layers,” *Surf. Coatings*

Technol., vol. 157, pp. 128–137, 2002.

[34] N. Cinca, E. López, S. Dosta, and J. M. Guilemany, "Study of stellite-6 deposition by cold gas spraying," *Surf. Coatings Technol.*, vol. 232, pp. 891–898, 2013.

[35] R. Singh, D. Kumar, S. K. Mishra, and S. K. Tiwari, "Laser cladding of Stellite 6 on stainless steel to enhance solid particle erosion and cavitation resistance," *Surf. Coatings Technol.*, vol. 251, pp. 87–97, 2014.

[36] J. Shin, J. Doh, J.-K. Yoon, D. Lee, and J. Kim, "Effect of Mo on the microstructure and wear resistance of cobalt-base Stellite hardfacing alloys.pdf," *Surf. Coat. Technol.*, vol. 166, pp. 117–126, 2003.

[37] L. Giourntas, T. Hodgkiess, and A. M. Galloway, "Comparative study of erosion–corrosion performance on a range of stainless steels," *Wear*, vol. 332–333, pp. 1051–1058, 2015.

[38] H. Meng, X. Hu, and A. Neville, "A systematic erosion-corrosion study of two stainless steels in marine conditions via experimental design," *Wear*, vol. 263, pp. 355–362, 2007.

[39] A. Neville and C. Wang, "Erosion-corrosion of engineering steels-Can it be managed by use of chemicals?," *Wear*, vol. 267, no. 11, pp. 2018–2026, 2009.

[40] ASTM International, "G59-97 - Standard test method for conducting potentiodynamic polarization resistance measurements," 2014.

[41] X. Yangtao, X. Tiandong, and H. Yanling, "Microstructures Comparison of Stellite 6 Alloy by Self-Propagating High-Temperature Synthesis and Cast HS111 Alloy," *Rare Met. Mater. Eng.*, vol. 38, no. 8, pp. 1333–1337, 2009.

[42] R. J. Llewellyn, S. K. Yick, and K. F. Dolman, "Scouring erosion resistance of metallic materials used in slurry pump service," *Wear*, vol. 256, no. 6, pp. 592–599, 2004.

[43] S. A. Romo, J. F. Santa, J. E. Giraldo, and A. Toro, "Cavitation and high-velocity slurry erosion resistance of welded Stellite 6 alloy," *Tribol. Int.*, vol. 47, pp. 16–24, 2012.